Available online at www.sciencedirect.com
SCIENCE DIRECT
Polymer 47 (2006) 679–689
polymer
www.elsevier.com/locate/polymer

Temperature dependence of crack initiation fracture toughness of various nanoparticles filled polyamide 66

Hui Zhang [a], Zhong Zhang [a,b,*], Jing-Lei Yang [a], Klaus Friedrich [a]

[a] *Institute for Composite Materials, University of Kaiserslautern, 67663 Kaiserslautern, Germany*
[b] *National Center for NanoScience and Technology, No. 2, 1st North Street Zhongguancun, 100080 Beijing, China*

Received 31 July 2005; received in revised form 9 November 2005; accepted 18 November 2005

Abstract

In the present study, the crack initiation fracture toughness of various nanoparticles filled polyamide 66 was investigated in a broad temperature range (23–120 °C) by using an essential work of fracture (EWF) approach. Four types of spherical nanoparticles, i.e. two types of TiO_2 (21 nm, with/without surface modification), SiO_2 (13 nm) and Al_2O_3 (13 nm), were selected with a constant volume content of 1% in nanocomposites, which were compounded using a twin-screw-extruder. The addition of nanoparticles led to an enhanced specific EWF item at most test temperatures at the cost of the reduction of the non-EWF item. The value of the specific EWF was also estimated by a crack opening displacement method. Associated with SEM fractograph analysis, it was clear that two basic factors, i.e. crack tip blunting and net section stress, finally determined the EWF value. With the addition of nanoparticles, the item of crack tip blunting was increased at most temperature range, which may be incidental with the formation of numerous dimples and sub-dimples induced by nanoparticles; while the item of net section stress was correlated with the particle distribution, especially at room temperature, which was notably decreased in case of poor nanoparticle distribution.

Keywords: Thermoplastic; Toughening; Temperature dependence

1. Introduction

It was reported [1–3] that rigid inorganic particles are able to enhance both the toughness and stiffness of some semicrystalline thermoplastics simultaneously. The fracture toughness of thermoplastics could be dramatically increased by introducing the rigid particles with typical volume content of 10–35%. Many possible toughening mechanisms were proposed. Generally speaking, two categories can be mainly considered, i.e. the crack front bowing and the cavitation mechanisms [4]. It is worth to note that the size of aforementioned rigid particles varies usually from sub- to several microns. However, if the particle size reduces to a nanometre scale, the toughening mechanisms would be obviously different, which is likely due to the huge particle–matrix interface introduced by the nanofillers. Toughness of rigid nanoparticle filled polymers deserves a separate treatise due to some contradictory findings in literatures. Corresponding toughening mechanisms induced by nanoparticles have not yet been well understood. Lots of factors (particle size, shape, distribution, type, aspect ratio, interface, particle concentration, and dispersion, etc.) may strongly affect the toughening efficiency of nanoparticles. To our knowledge, nanoparticles with a high aspect ratio, e.g. clay, often bring negative toughening effects. It is because under external load the large aspect ratio will generate significantly high stress concentrations at the end of the particles, which lead to earlier crack initiation and propagation, and finally are adverse to material toughness [5]. Chen et al. reported that the *J*-integral value of polypropylene (PP) decreased significantly with an increase of clay filler content [6]. Bureau et al. [7] found that the addition of clay (with/without coupling agents) into PP matrix reduced the specific essential fracture work, w_e, but increased the specific non-essential fracture work item, (βw_p. The quasi-spherical nanoparticles were recognized to be more promising for polymer toughening. Chan et al. [8] conducted very tough PP/$CaCO_3$ nanocomposites by melt mixing, and the *J*-integral tests showed a dramatic 500% increase in fracture toughness. Our previous work [9] indicated also that only 1–3 vol% nano-TiO_2 can notably enhance the fracture work of resistance to crack initiation at room temperature.

* Corresponding author. Address: National Center for NanoScience and Technology, No. 2, 1st North Street Zhongguancun, 100080 Beijing, China.
E-mail address: zhong.zhang@nanoctr.cn (Z. Zhang).

0032-3861/$ - see front matter © 2005 Elsevier Ltd. All rights reserved.
doi:10.1016/j.polymer.2005.11.084

PA66 is a semicrystalline thermoplastic polymer used for numerous engineering applications due to its combination of high thermal and mechanical properties with easy processing and moderate cost. However, neat PA66 is notch sensitive and sometimes tends to be broken in a brittle fashion. The deficiency has somewhat limited its broad utilities [10]. Besides, many automotive parts made of PA-based composites are required to be operated at elevated temperatures [11]. Therefore, their high-temperature mechanical performances, especially fracture toughness, should be taken into consideration. In this study, temperature dependent fracture properties of PA66 and its nanocomposites filled with different types of nanoparticles will be carried out. An essential work of fracture (EWF) approach with deeply double edge notched tensile (DDENT) specimens was applied. The EWF parameters were also estimated and analyzed via a crack opening displacement (COD) method, and the fracture surfaces were observed by a scanning electron microscope (SEM). In light of the experimental results and COD method, the related fracture mechanisms were further discussed.

2. Methodology of the essential work of fracture

The essential work of fracture (EWF) approach, firstly proposed by Broberg [12–14], has been used to characterize the plane-stress-state fracture toughness of ductile materials, including metals, papers, polymers, fibre composites and even foods [15]. The EWF method has gained popularity owing to its experimental simplicity, especially compared to *J*-integral technique. Many reports have indicated that the EWF parameters are affected by a number of factors, such as sample geometry [16–20], test conditions [21–25], notching method [26,27], polymer composition [28,29], filler fraction [30–32] and so on [33–36]. Recently, this method has been introduced to investigate the toughening effects of polymer nanocomposites as well [7,9,37]. A brief review of the EWF method was given in our previous paper [9], where we divided total dissipated energy (W_f) into two items, i.e. crack initiation (W_{ini}) and subsequent crack propagation (W_{prop}), respectively, according to the energy-partitioned method proposed by Karger-Kocsis [38] and Hashemi [23]. As schematically depicted in Fig. 1(a), W_f can be expressed as:

$$W_f = W_{ini} + W_{prop} \tag{1}$$

As the continuation of our previous work, the present work still concentrated on the parameter W_{ini}, since it represents the fracture energy consumed at crack initiation stage and is a crucial parameter for material design in engineering applications. Based on the EWF concept, W_{ini} is considered as a sum of essential and non-essential work of facture. The specific item (w_{ini}) can be described as:

$$w_{ini} = \frac{W_{ini}}{lt} = w_{e,ini} + \beta_{ini} w_{p,ini} l \tag{2}$$

where $w_{e,ini}$ and $w_{p,ini}$ are the specific essential and non-essential work of fracture related to crack initiation,

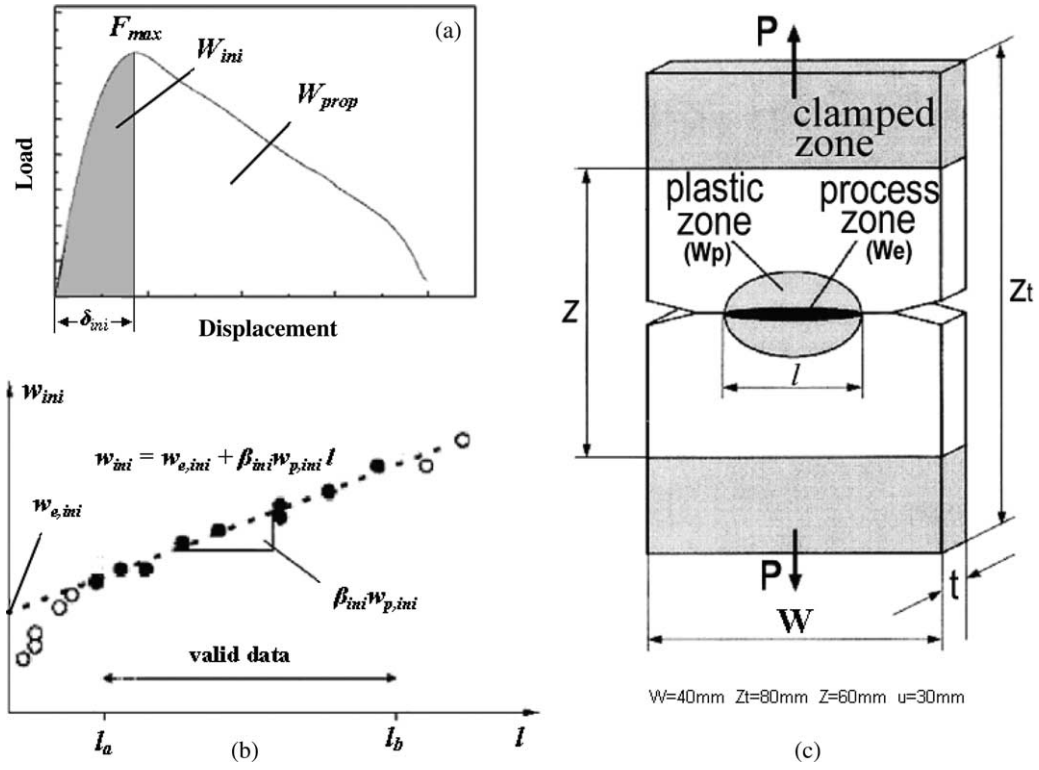

Fig. 1. Schematic diagram of the essential work of fracture (EWF) approach: (a) a typical load–displacement curve; (b) a curve of specific total work of fracture vs. ligament length; and (c) the dimensions of the deeply double edge notched tensile (DDENT) specimens.

respectively. β_{ini} is the shape factor. l and t symbolize the ligament length and thickness of specimen, respectively. According to Eq. (2), the specific essential and non-essential work of fracture ($w_{e,ini}$ and $\beta_{ini}w_{p,ini}$) can be obtained from linear regression of a set of values represented in a diagram of w_{ini} vs. l (Fig. 1(b)).

Furthermore, the specific essential work of fracture can be straightforwardly estimated via crack opening displacement (COD) approach proposed by Hashemi et al. [23]. Assuming that load–displacement curve of DDENT specimen (Fig. 1(a)) is parabolic in shape, the following equation can be easily deduced:

$$w_{e,ini} = \frac{2}{3}\sigma_{net}\delta_{0,ini} \tag{3}$$

where $\sigma_{net}(=F_{max}/lt)$ is the net section stress of a DDENT specimen; $\delta_{0,ini}$ is the COD related to crack initiation, which is the extrapolated value of δ_{ini} at $l=0$ according to Eq. (4):

$$\delta_{ini} = \delta_{0,ini} + \alpha_{ini}l \tag{4}$$

where δ_{ini} is the displacement related to crack initiation (Fig. 1(a)), and α_{ini} is the corresponding proportional constant.

3. Experimental

3.1. Material preparation

Commercial PA66 (DuPont Zytel 101) was used as matrix, and four types of nanoparticles were applied as fillers in this study. These particles were TiO_2 (with/without surface modification), SiO_2 and Al_2O_3 nanoparticles, which were all supplied by Degussa. Detailed characteristics of the nanoparticles are listed in Table 1. Prior to compounding, PA66 and nanoparticles were dried in an oven at 70 °C for about 72 h. Compounding of the matrix and nanoparticles was carried out in a co-rotating twin-screw extruder (Berstoff ZE 25A×44D-UTS) with well-designed screw elements. The barrel temperatures were set as 55/260/270/280/285/285/285/285/285 °C, and the screw speed was 150 rpm. During melt extrusion, ventilation was kept on to remove trapped air in blends. After extrusion, the blend granules were injection-moulded into 2 mm-thick plates for EWF tests using an injection-moulding machine (Alburg Allrounder 320S). For all samples, the parameters of injection moulding were maintained constantly. The barrel temperature ranged from 280 to 295 °C and the mould temperature was kept at 70 °C. The injection pressure and speed were 500 bar and 80 cm^3/s, respectively. The nanoparticle content was set constant as 1 vol%. A detailed description of PA-based nanocomposites is given in Table 1 additionally.

3.2. Property investigation

The thermo-grams of all samples were carried out on a DSC821 apparatus (METTLER TOLEDO). All tests were performed in nitrogen atmosphere with a sample mass of about 17–18 mg. The scanning rate was 10 °C/min. To completely eliminate thermal history, the sample was held at 300 °C for 3 min, and then cooled down to 50 °C at the same scanning rate. The crystallinity of sample (X_c) was calculated according to Eq. (5):

$$X_c = \frac{\Delta H_m}{\Delta H_m^0(1-w_t)} \tag{5}$$

where ΔH_m is the specific melting heat, ΔH_m^0 is the theoretical specific melting heat of 100% crystalline PA66, which is taken to be 195 J/g, and w_t is the weight fraction of nanoparticles. Note that the surface modifier of nanoparticles can be negligible due to its minute weight fraction in the composites.

DMTA was performed by using a Gabo Qualimetrer Explexor 25N under tension mode. The dynamic complex modulus and loss factor of specimen ($55\times10\times2$ mm^3) were determined at a constant frequency of 10 Hz in a temperature range of 0–180 °C at a heating rate of 2 °C/min.

EWF tests were carried out on DDENT specimens with dimensions shown in Fig. 1(c). The pre-crack was made by slowly pushing a fresh razor blade into the bottom of saw slot. In order to satisfy the state of plane stress, the ligament length of the specimen ranged from 6 to 13 mm. Quasi-static tensile tests were performed on a universal testing machine (Zwick 1485) at a constant crosshead speed of 1 mm/min. The displacement of each specimen during tension was accurately measured by an extensometer. After tests a light microscope was used to measure the ligament length and the average value was used for each specimen. The specific essential and non-essential work of fracture were obtained from linear regression equation as mentioned earlier. The data were processed according to the ESIS protocol [39]. At least 20 specimens were tested for each composition. The fracture surfaces sputtered with gold films were examined by a scanning electron microscope (SEM, JEOL 5400).

Table 1
Detailed information on nanoparticles and PA-based nanocomposites

Sample designation	Nanoparticle type	Volume fraction (%)	Nanoparticle designation	Particle diameter (nm)	Particle density (g/cm^3)	Specific surface area (BET)	Surface modification
Neat PA	–	–	–	–	–	–	–
1TPA	TiO_2	1	P25	21	4.0	50±15	None
1T805PA	TiO_2	1	T805	21	4.0	45±10	Ostylsilane
1R7200PA	SiO_2	1	R7200	13	2.2	150±25	Methacrysilane
1APA	Al_2O_3	1	Aluminiumoxide C	13	2.9	100±15	None

Table 2
DSC and DMTA results of PA-based nanocomposites

Sample designation	DSC			DMTA	
	X_c (%)	T_m (°C)	T_c (°C)	T_g (°C)	tan δ_{max}
Neat PA	38.67	266.34	232.31	59.7	0.123
1TPA	34.53	266.45	232.70	71.6	0.133
1T805PA	38.56	266.26	232.51	67.5	0.127
1R7200PA	37.94	266.60	233.84	69.8	0.127
1APA	35.68	265.35	233.53	69.8	0.141

4. Results and discussion

4.1. Thermal properties

DSC results are summarised in Table 2. It can be seen that the small amount of nanoparticles did not affect the crystallinity degree (X_c), the melting point (T_m) as well as the crystallization temperature (T_c) of the host matrix. Therefore, the influence of crystallinity on the matrix toughness by introducing the nanoparticles was negligible.

Fig. 2 presents the DMTA results. The glass transition temperature (T_g) and the peak value of loss factor (tan δ_{max}) listed in Table 2 are the average values calculated from two measurements of each sample. It is observed that, by introducing only 1 vol% nanoparticles, T_g was shifted to higher temperature by about 10 °C, while the tan δ_{max} was slightly changed with respect to neat PA. The results confirmed that small amount of nanoparticles can effectively restrain the movements of polymeric chain segments, which in turn affected the matrix toughness, especially in the regions near the glass transition temperature. And this will be discussed in the following sections.

4.2. Essential work of fracture (EWF)

Load–displacement (F–δ) curves of DDENT specimens were obtained at various test temperatures. Most specimens exhibited full ductile fracture in the whole temperature range. Large plastic deformation zone surrounding crack tip and evident necking after yielding were clearly observed when the specimens were loaded. The typical F–δ curves are shown in Fig. 3(a) for PA66 with 1 vol% TiO_2 (1T805PA) measured at room temperature. These F–δ curves were geometrical similarity, which indicated that fracture mechanism was probably independent on the ligament length. Actually, the self-similarity of F–δ curves is a basic precondition of the EWF methodology to be applied. Fig. 3(b) illustrates the typical F–δ curves at various temperatures of 1T805PA at a constant ligament length ($l \approx 10$ mm). It can be found that for a given ligament length, with increasing temperature, the maximum

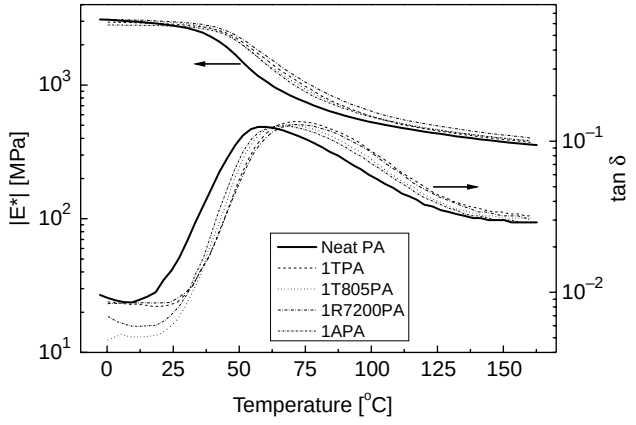

Fig. 2. Dynamic mechanical thermal analysis curves of loss factor and dynamic complex modulus against temperature.

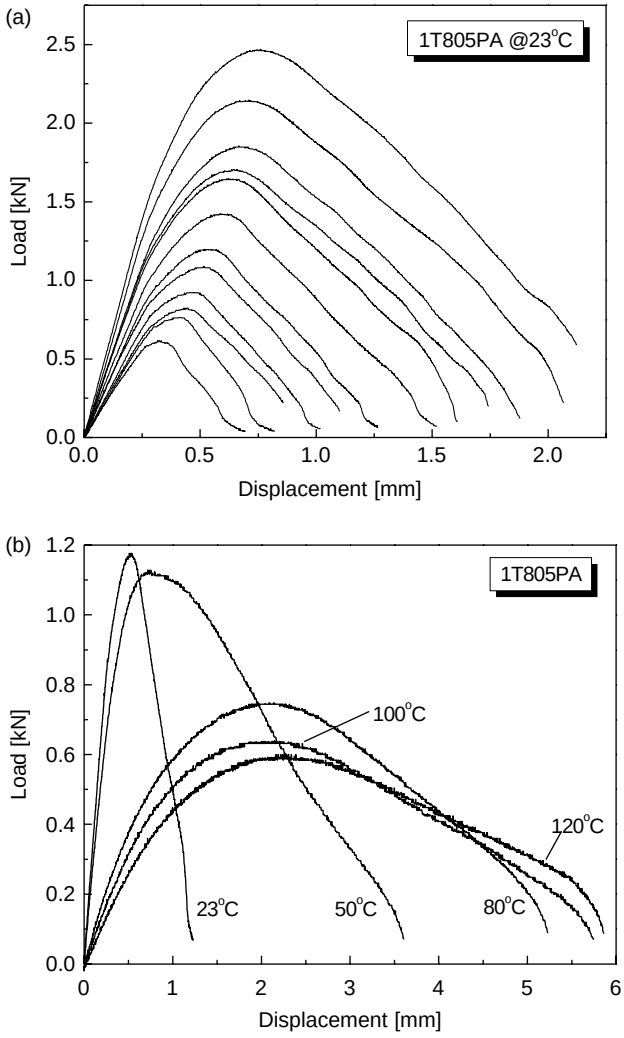

Fig. 3. Typical load–displacement curves of the nanocomposites studied: (a) 1T805PA at 23 °C with different ligament length; and (b) 1T805PA at various temperatures with a constant ligament length (≈10 mm).

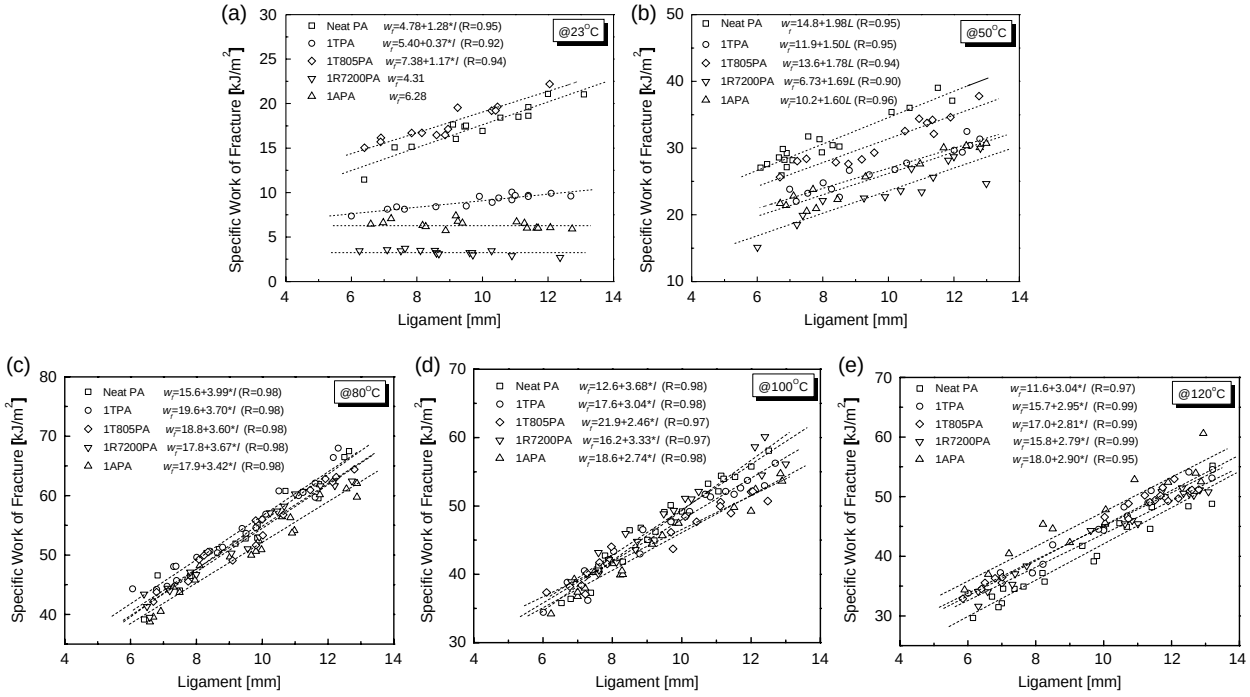

Fig. 4. Curves of the specific work of fracture related to crack initiation against the ligament length of DDENT specimens: (a) 23 °C; (b) 50 °C; (c) 80 °C; (d) 100 °C; and (e) 120 °C.

load decreased, but the displacement at break extended. Fig. 4 presents the w_{ini} vs. l curves for all samples measured at various temperatures. It can be seen that for the great majority of samples, positive slopes and good linear correlation coefficients ($R>0.9$) can be obtained. The corresponding EWF parameters, i.e. $w_{e,ini}$ and $\beta_{ini}w_{p,ini}$, which represent respectively the resistance to crack initiation and the contribution of plastic zone to the crack resistance, can be acquired from intercepts and slopes of linear regression equations. However, it is also noticed that two groups of samples (1R7200PA and 1APA) exhibited semi-ductile fracture at room temperature, i.e. unstable fracture occurred after yielding. And the specific work of fracture was nearly constant to the ligament length on the w_{ini} vs. l curve (Fig. 4(a)). In other words, the specific non-essential work item for fracture initiation ($\beta_{ini}w_{p,ini}$) can be set to zero for these two samples. And hence the $w_{e,ini}$ values can be straightforwardly obtained from the intercepts of the horizontal dash lines in Fig. 4(a). A similar approach was applied by Mai and Cotterell [15] on polymer materials when using the work of fracture methodology. All these results are summarised in Table 3 additionally.

4.3. Temperature dependence of EWF parameters

Temperature dependence of EWF parameters of ductile materials was studied by many researchers. Previous work done by Wu et al. [28] indicated that both static and impact fracture toughness of PBT/PC/IM (impact modifier) blends had respectively the maximum values at certain temperatures. Hashemi et al. [23–25] studied a series of polymer films at various temperatures and found both $w_{e,ini}$ and $\beta_{ini}w_{p,ini}$ decreased more or less with increasing temperature. However, it should be noted that the test temperatures used in their studies were always below the glass transition temperatures of the corresponding materials.

The temperature dependence of the EWF parameters ($w_{e,ini}$ and $\beta_{ini}w_{p,ini}$) of PA66 and its nanocomposites are given in Fig. 5. Generally speaking, both $w_{e,ini}$ and $\beta_{ini}w_{p,ini}$ increased at elevated temperature for all materials in the present work. It can be seen that $w_{e,ini}$ of the neat PA66 exhibited a peak value in the range between 50 and 80 °C; however, this trend was different for the nanocomposites, which showed the peak values at around 80 and 100 °C. Regarding the toughening effects, the addition of nanoparticles, on the one hand, improved the $w_{e,ini}$ value of the host matrix at most test temperatures. The only exception at 50 °C was likely due to the influence of glass transition on polymer toughness, which will be further discussed in the next paragraph. On the other hand, various nanoparticles reduced the $\beta_{ini}w_{p,ini}$ value of the host matrix in the whole temperature range, which indicated that the ability to plastic deformation of matrix was decreased after adding the nanoparticles. In other words, the incorporation of rigid nanoparticles improved the resistance to crack initiation at the cost of the reduced resistance to crack propagation in the measured temperature range. This finding is also in agreement with the previous claim [38] that these two EWF parameters cannot be improved simultaneously.

As shown in Fig. 5(a), the peak values of crack resistance existed near glass transition temperature (T_g) of the studied samples, which implied some relationship between crack initiation toughness and polymeric segment relaxation. It is known that in the vicinity of T_g, parts of polymeric segments absorbed enough energy and started to move, however, the very tight moving space between the macromolecules caused

Table 3
EWF parameters of PA-based nanocomposites at various temperatures

Sample designation	Temperature (°C)	σ_{net}(MPa)	$\delta_{0,ini}$ (mm)	$w_{e,ini}$ (kJ/m^2) (estimated)	$w_{e,ini}$ (kJ/m^2) (experimental)	$\beta_{ini}w_{p,ini}$ (MJ/m^3) (experimental)
Neat PA	23	57.6	0.18	6.95	4.78	1.28
	50	57.9	0.38	14.7	14.8	1.98
	80	36.1	0.53	12.8	15.6	3.99
	100	31.6	0.70	14.6	12.6	3.68
	120	30.2	0.72	14.4	11.6	3.04
1TPA	23	46.1	0.16	4.94	5.40	0.37
	50	56.7	0.29	11.0	11.9	1.50
	80	37.1	0.72	17.9	19.6	3.70
	100	32.5	0.95	20.7	17.6	3.04
	120	29.9	0.99	19.5	15.7	2.95
1T805PA	23	57.9	0.23	8.92	7.38	1.17
	50	58.3	0.40	15.6	13.6	1.78
	80	37.8	0.71	18.0	18.8	3.60
	100	32.6	1.03	22.5	21.9	2.46
	120	29.2	1.03	19.9	17.0	2.81
1R7200PA	23	29.8	0.19	3.80	4.31	0
	50	49.8	0.26	8.68	6.73	1.69
	80	38.5	0.79	20.4	17.8	3.67
	100	34.0	0.92	20.9	16.2	3.33
	120	31.3	0.95	19.6	15.8	2.79
1APA	23	38.5	0.24	6.19	6.28	0
	50	53.7	0.31	11.2	10.2	1.60
	80	37.4	0.62	15.5	17.9	3.42
	100	32.8	0.90	19.8	18.6	2.74
	120	30.9	1.01	20.6	18.0	2.90

the high internal friction, thus an additional energy was required for molecule movements [40]. That was the reason why all samples exhibited peak values of loss factor near T_g, as shown in Fig. 2. Such additional energy consumption near T_g was believed to be of benefit to the fracture toughness as well. Comparing the DMTA curve in Fig. 2 with the crack initiation toughness curve in Fig. 5(a), one can find that the two curves displayed approximately similar tendency, even though the latter was not continuous. Therefore, it can be inferred from above discussion that the shift of the peak values of $w_{e,ini}$ of the nanocomposites to higher temperatures was probably due to the increased T_g by nanoparticles.

4.4. COD analysis

In order to understand the toughening mechanisms of the nanocomposites, a crack opening displacement (COD) approach was introduced. In Eq. (3), $w_{e,ini}$ can be considered as a product of two basic items, i.e. $\delta_{0,ini}$ and σ_{net}. Here $\delta_{0,ini}$ represents the degree of crack tip blunting during crack initiation process, and σ_{net} correlates with material yielding stress (according to plasticity theory, $\sigma_{net}=1.15\sigma_y$ for DDENT specimen under pure plane stress condition [25]). Both $\delta_{0,ini}$ and σ_{net} were calculated and summarised in Table 3. Thereafter, the $w_{e,ini}$ values were estimated by Eq. (3) and plotted in Fig. 6. To compare Fig. 6 with Fig. 5(a), it can be recognized that the estimated $w_{e,ini}$ values with the COD method roughly corresponded with the experimental results.

Temperature dependence of both $\delta_{0,ini}$ and σ_{net} of the various nanocomposites are given in Fig. 7. The general tendency in Fig. 7(a) shows that the addition of nanoparticles can more or less reduce σ_{net} values of the host matrix. The difference of the σ_{net} item between the matrix and nanocomposites was much more obvious at room temperature, while it was gradually diminished with increasing temperature. However, the situation was different for the crack tip blunting, $\delta_{0,ini}$, as shown in Fig. 7(b). The addition of nanoparticles increased the $\delta_{0,ini}$ value at most test temperatures. The abnormally high $\delta_{0,ini}$ of the neat matrix at 50 °C was again due to the influence of polymeric segment relaxation near T_gs, as discussed in earlier section.

In addition, it is easy to understand from Eq. (3) that after introducing the nanoparticles, once the increase in $\delta_{0,ini}$ outweighs the decrease in σ_{net}, the $w_{e,ini}$ value will increase, and vice versa. Therefore, the variation of $\delta_{0,ini}$ and σ_{net} with temperature is important to the understanding of the toughening mechanisms of nanocomposites. It was also found from Fig. 7 that at room temperature both $\delta_{0,ini}$ and σ_{net} dominated the final $w_{e,ini}$ value. However, at elevated temperatures, the influence of σ_{net} turned into much minor. Thus the gradually increased $\delta_{0,ini}$ became the dominating item to $w_{e,ini}$.

4.5. SEM fractograph

SEM fractographs of the specimens studied offered much information on the toughening mechanisms and may partially explain the variations of the $\delta_{0,ini}$ and σ_{net} values after addition of nanoparticles. The fractographs of the neat PA66 and various nanocomposites measured at room temperature are

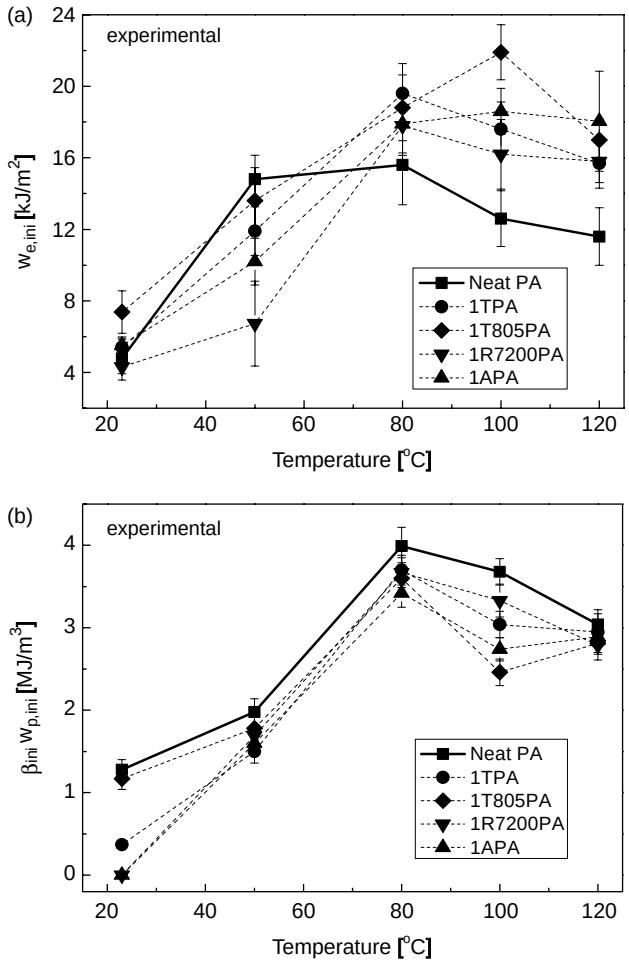

Fig. 5. Temperature dependence of (a) $w_{e,ini}$ (specific essential work of fracture) and (b) $\beta_{ini} w_{p,ini}$ (specific non-essential work of fracture item).

illustrated in Fig. 8. Numerous dimples can be found near crack tips for all specimens. However, the size, ranged approximately from 20 to 100 μm, and density of these dimples strongly depend on the types of nanoparticles. Our previous work [9] indicated that under load, nuclei of spherulites, matrix defects, nanoparticles and their aggregates could serve as stress concentrators in matrix, promoting formation of these dimples. A higher resolution fractograph in Fig. 9(b) further shows that tiny structures in hyperbolic shapes existed on the walls of these dimples of the nanocomposites (termed as 'sub-dimple', marked by black arrows in Fig. 9(b)). The structure is certainly correlated with stress concentrations of single nanoparticle or smaller aggregates. By contrast, no such sights can be found for the neat matrix, the walls of its dimples were much smooth, as given in Fig. 9(a). It is believed that formation of these dimples and sub-dimples of nanocomposites is accompanied by a series of energy dissipative events, such as localized micro-deformation of matrix, particle debonding, and cavitations. All these events may reduce the stress intensity or modify the stress state around the crack tip, which contribute to an increased blunting of the crack tip, $\delta_{0,ini}$. Therefore, high-density dimples might directly correspond to high degree of crack tip blunting. The crack tip blunting effect of the

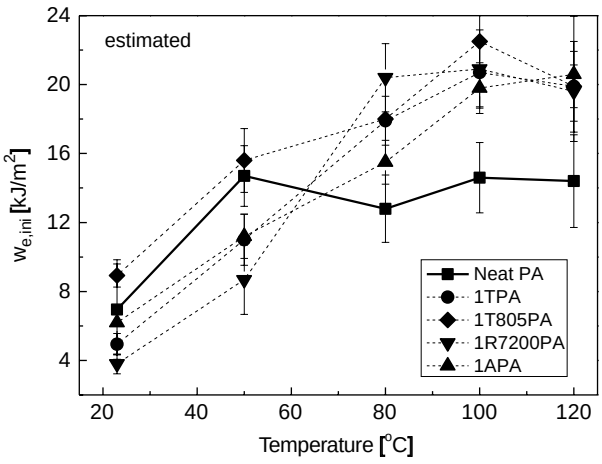

Fig. 6. Temperature dependence of the estimated specific essential work of fracture ($w_{e,ini}$).

nanocomposites was generally higher than that of the neat matrix at the most test temperature range (Table 3). And such speculation was further evidenced by the fractographs at elevated temperatures, as shown in Figs. 10 and 11. Again, high-density dimples were always accompanied by the higher values of $\delta_{0,ini}$. It should be noticed that at 120 °C the composites became relatively soft, thus the dimples were

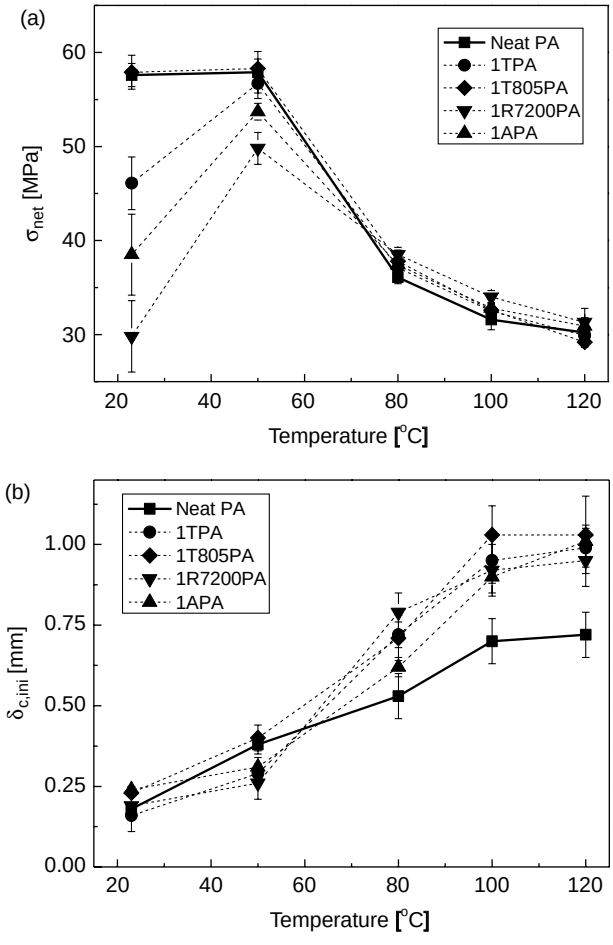

Fig. 7. Temperature dependence of (a) σ_{net} (crack tip blunting) and (b) $\delta_{0,ini}$ (net section stress).

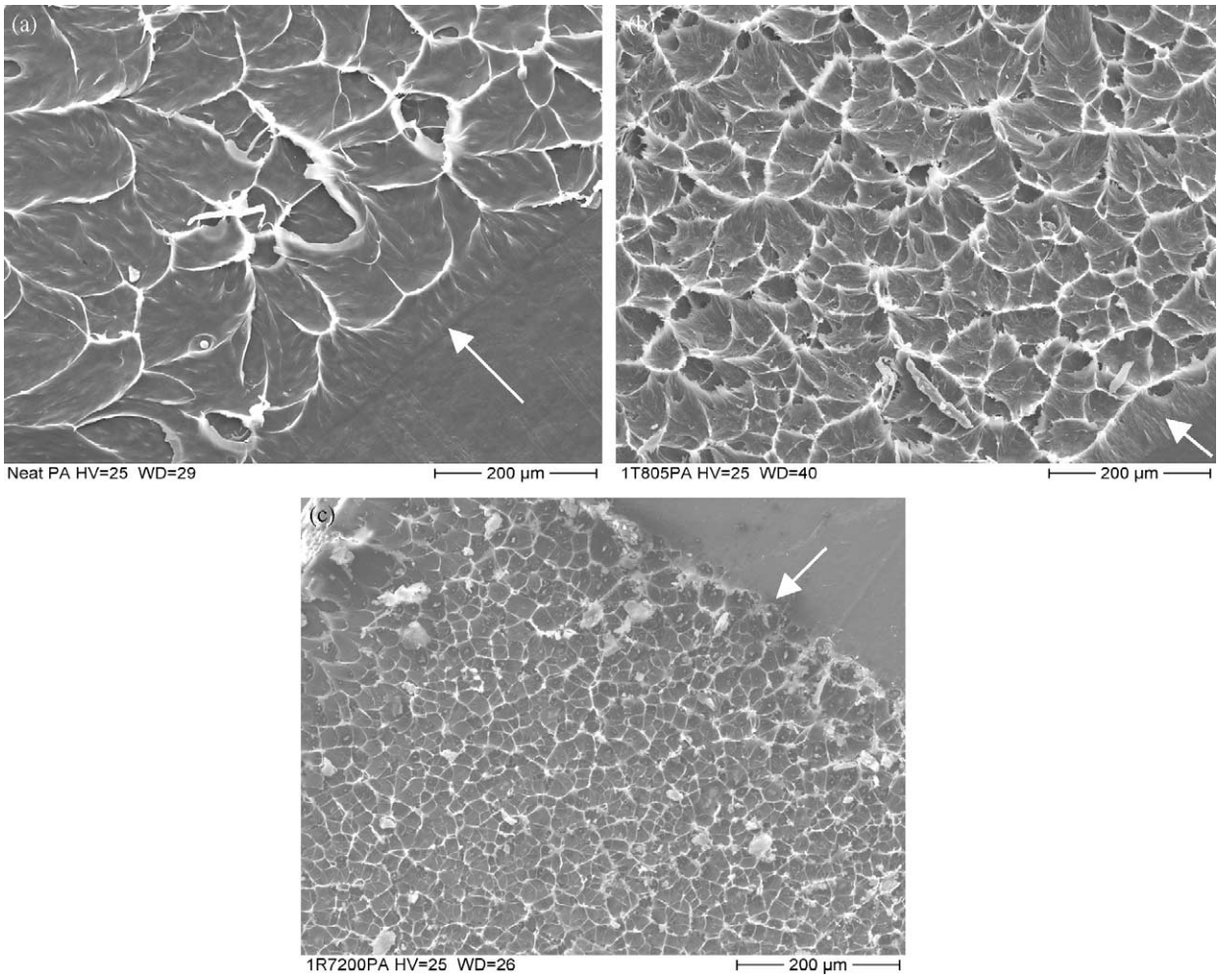

Fig. 8. Typical SEM fractographs of DDENT samples at 23 °C: (a) neat PA; (b) 1T805PA; and (c) 1R7200PA. The arrows indicate the pre-crack tips.

extremely stretched and oriented along the crack propagation direction (Fig. 11).

On the other hand, as discussed in Section 4.4, the addition of nanoparticles could reduce the σ_{net} item, especially at room temperature. It was found that normally this reduction was associated with the relatively poor nanoparticle dispersion. For example, Fig. 9(b) presents a better dispersion of nano-TiO_2 on the fracture surface of 1T805PA. The reason was likely due to the lowest specific surface area of the nano-TiO_2 among all the nanoparticles as well as the appropriate surface modifier used (Table 1). Correspondingly, the σ_{net} value of 1T805PA changed slightly compared to the neat matrix. By contrast,

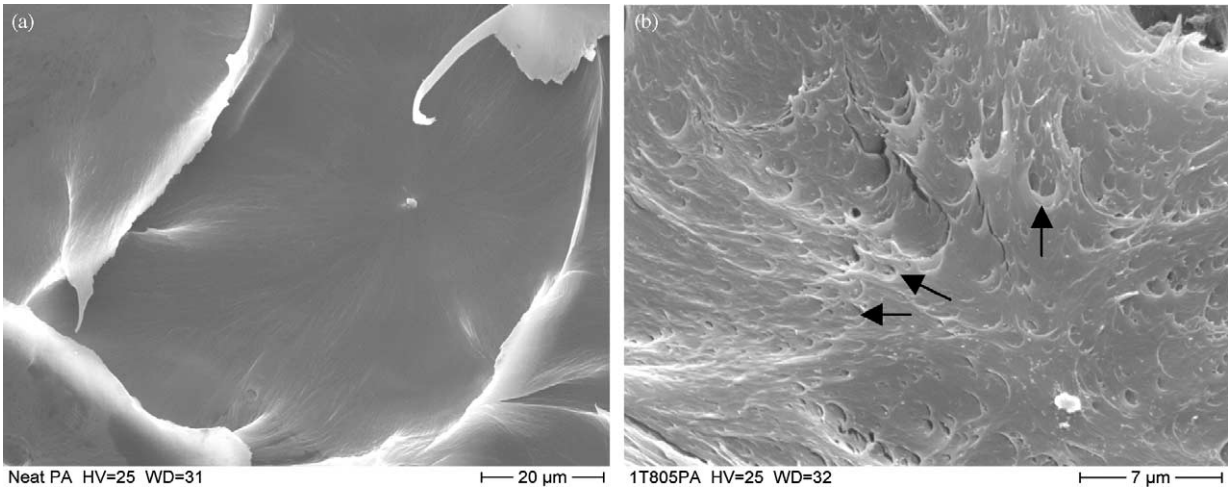

Fig. 9. Close-up of a dimple of DDENT samples at 23 °C: (a) neat PA; and (b) 1T805PA.

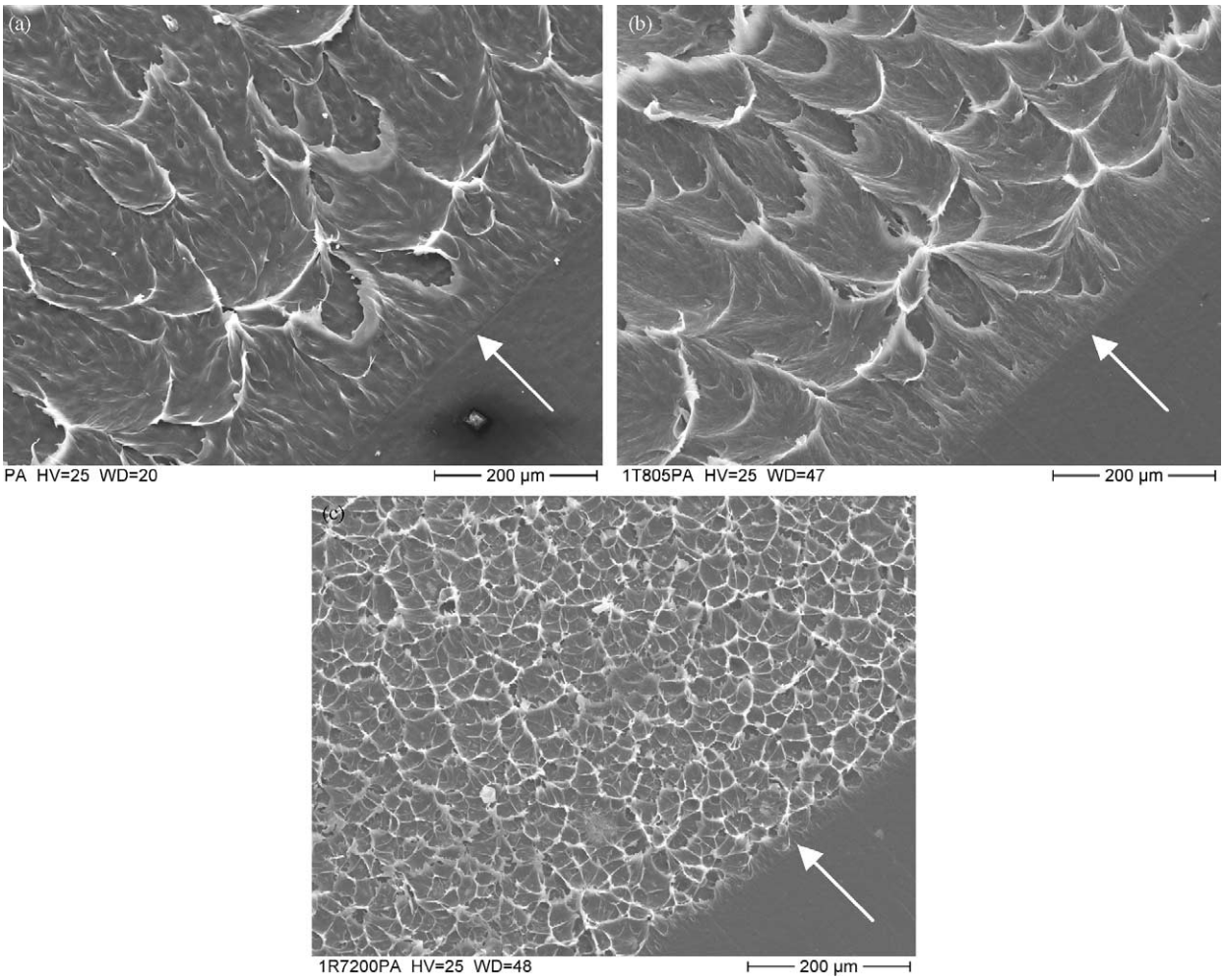

Fig. 10. Typical SEM fractographs of DDENT samples at 50 °C: (a) neat PA; (b) 1T805PA; and (c) 1R7200PA. The arrows indicate the pre-crack tips.

some large aggregates can be observed on the fracture surfaces of 1R7200PA composite (as shown in Fig. 8(c)). These large aggregates may act as defects, triggering the premature cracks, and finally decreasing the σ_{net} value. As a result, 1R7200PA presented a very low σ_{net} at room temperature in comparison with the neat matrix. However, at elevated temperatures, the premature fracture cannot be formed as easily as at room temperature, and the influence of σ_{net} turned into much minor for all materials.

5. Conclusions

In this study, temperature dependence of the crack initiation fracture toughness of various nanoparticles filled PA66 composites was investigated based on an essential work of fracture approach. The following conclusions can be drawn:

(1) The addition of a very small amount of nanoparticles (1 vol%) did not obviously alter the melting temperature, the crystallizing temperature and the crystallinity of the host matrix, while it effectively increased the glass transition temperature of matrix by about 10 °C, which suggested the strong interactions between nanoparticles and the matrix.

(2) EWF parameters ($w_{e,ini}$ and $\beta_{ini}w_{p,ini}$) strongly depended on test temperatures, and exhibited peak values at certain temperature range. In general, at most test temperatures the addition of nanoparticles resulted in positive toughening effects (i.e. increased $w_{e,ini}$ item) with the cost of the reduction in plastic deformation of matrix (i.e. decreased $\beta_{ini}w_{p,ini}$ item). The influence on fracture toughness of the additional energy consumption around T_g should be also taken into account for the materials studied.

(3) Based on COD analysis and SEM fractographs, two factors, i.e. crack tip blunting ($\delta_{0,ini}$) and net section stress (σ_{net}), were found to be related to the crack initiation fracture toughness ($w_{e,ini}$) of the nanocomposites. $\delta_{0,ini}$ can be enhanced at most temperature range after the addition of various nanoparticles, probably due to the induced numerous dimples and sub-dimples. While, σ_{net} highly reflected to nanoparticle dispersion. Large aggregates of nanoparticles can significantly reduce the σ_{net} value, especially at room temperature; however, this trend was diminished at increased temperature.

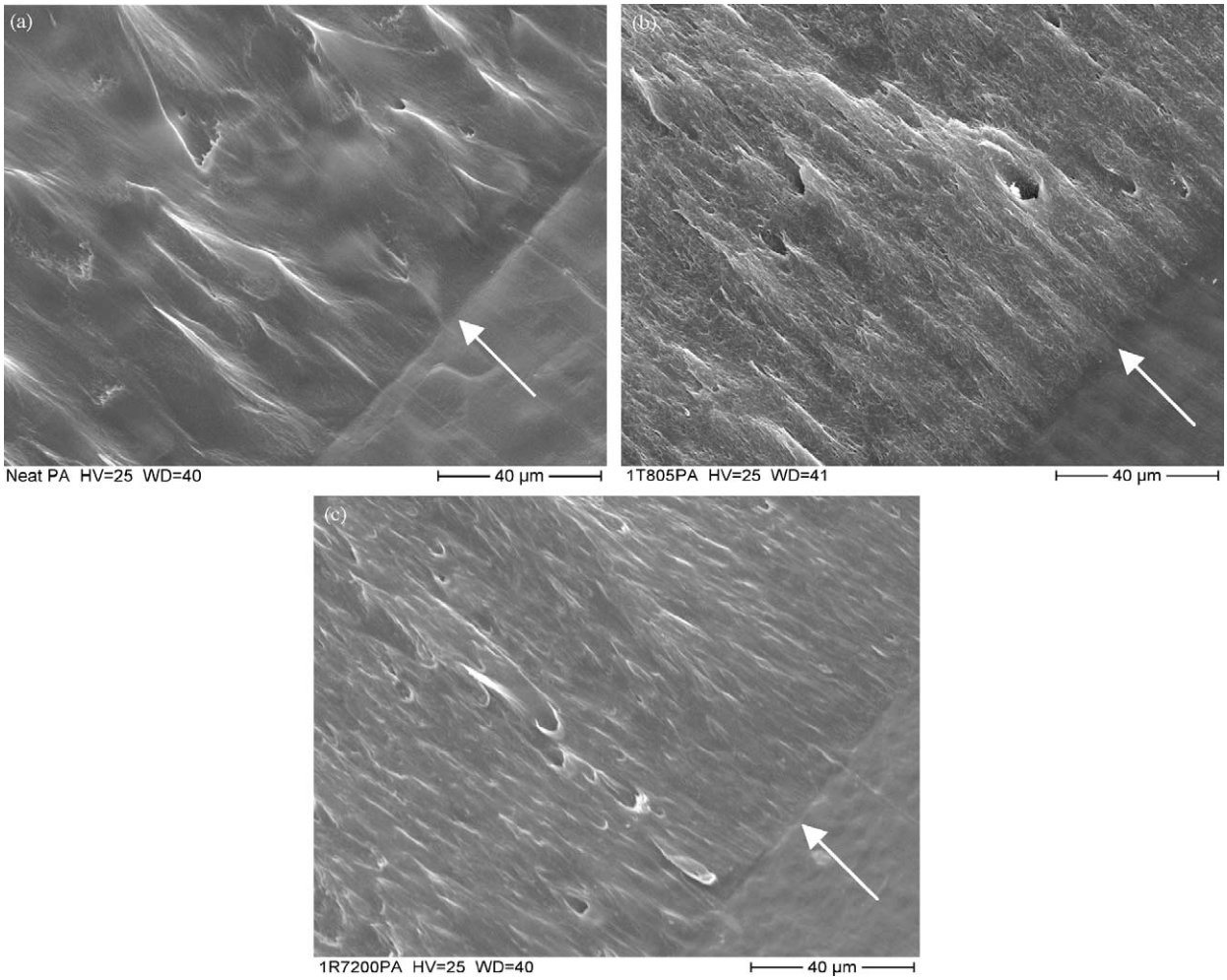

Fig. 11. Typical SEM fractographs of DDENT samples at 120 °C: (a) neat PA; (b) 1T805PA; and (c) 1R7200PA. The arrows indicate the pre-crack tips.

Acknowledgements

Z. Zhang is grateful to the Alexander von Humboldt Foundation for his Sofja Kovalevskaja Award, financed by the German Federal Ministry of Education and Research (BMBF) within the German Government's 'ZIP' program for investment in the future.

References

[1] Bartczak Z, Argon AS, Cohen RE, Weinberg M. Toughness mechanism in semi-crystalline polymer blends: II high-density polyethylene toughened with calcium carbonate filler particles. Polymer 1999;40: 2347–65.
[2] Wilbrink MWL, Argon AS, Cohen RE, Weinberg M. Toughenability of nylon-6 with $CaCO_3$ filler particles: new findings and general principles. Polymer 2001;42:10155–80.
[3] Argon AS, Cohen RE. Toughenability of polymers. Polymer 2003;44: 6013–32.
[4] Norman DA, Robertson RE. Rigid-particle toughening of glassy polymers. Polymer 2003;44:2351–62.
[5] Zuiderduium WCJ, Westzaun C, Huétink J, Gaymans RJ. Toughening of polypropylene with calcium carbonate particles. Polymer 2003;44: 261–75.
[6] Chen L, Wang S-C, Pisharath S. Fracture properties of nanoclay-filled polypropylene. J Appl Polym Sci 2003;88:3298–305.
[7] Bureau MN, Perrin-Sarazin F, Ton-That M-T. Polyolefin nanocomposites: essential work of fracture analysis. Polym Eng Sci 2004;44: 1142–51.
[8] Chan C-M, Wu J-S, Li J-X, Cheung Y-K. Polypropylene/calcium carbonate nanocomposites. Polymer 2002;43:2981–92.
[9] Yang J-L, Zhang Z, Zhang H. The essential work of fracture of polyamide 66 filled with TiO_2 nanoparticles. Compos Sci Technol 2005;65:2374–9.
[10] Kohan MI, Hewel M, Torre Dalla, et al. In: Kohan MI, editor. Nylon plastics handbook. Cincinnati: Hanser/Gardner Publication, Inc.; 1995. p. 414–34.
[11] Kim P, Schuh T, Wittig W. CFRP-from motor sports into automotive series: challenges and opportunities facing the technology transfer. Plast Autom Eng 2004;45–9.
[12] Broberg KB. Critical review of some theories in fracture mechanics. Int J Fract Mech 1968;4:11–18.
[13] Broberg KB. Discussion of initial and subsequent crack growth. Eng Fract Mech 1973;5:1031–5.
[14] Broberg KB. On stable crack growth. J Phys Mech Solids 1975;23: 215–37.
[15] Mai Y-W, Cotterell B. On the essential work of ductile fracture in polymers. Int J Fract 1986;32:105–25.
[16] Wu J-S, Mai Y-W. The essential fracture work concept for toughness measurement of ductile polymers. Polym Eng Sci 1996;36:2275–88.
[17] Hashemi S. Work of fracture of PBT/PC blend: effect of sample size, geometry and rate of testing. Polym Eng Sci 1997;37:912–21.
[18] Karger-Kocsis J, Czigany T, Moskala J. Thickness dependence of work of fracture parameters of an amorphous copolyester. Polymer 1997;38: 4587–93.

[19] Arkhirezeva A, Hashemi S, O'brien M. Factors affecting work of fracture of uPVC film. J Mater Sci 1999;34:5961–74.
[20] Hashemi S. Determination of the fracture toughness of polybutylene terephthalate (PBT) film by the essential work method: effect of sample size and geometry. Polym Eng Sci 2000;40:798–808.
[21] Low IT-M, Mai Y-W. Rate and temperature effects on crack blunting mechanisms in pure and modified epoxies. J Mater Sci 1989;24:1634–44.
[22] Karger-Kocsis J, Czigany T, Moskala J. Deformation rate dependence of the essential and non-essential work of fracture parameters in an amorphous copolyester. Polymer 1998;39:3939–44.
[23] Hashemi S, Williams JG. Temperature dependence of essential and non-essential work of fracture parameters for polycarbonate film. Plast Rubber Compos 2000;29:294–302.
[24] Arkhireyeva A, Hashemi S. Combined effect of temperature and thickness on work of fracture parameters of unplasticized PVC film. Polym Eng Sci 2002;42:504–18.
[25] Arkhireyeva A, Hashemi S. Effect of temperature on work of fracture parameters in poly(ether-ether ketone) (PEEK) film. Eng Fract Mech 2004;71:789–804.
[26] Poon WKY, Ching ECY, Cheng CY, Li RKY. Measurement of plane stress essential work of fracture (EWF) for polymer films: effects of gripping and notching methodology. Polym Test 2001;20:395–401.
[27] Yamakawa RS, Razzino CA, Correa CA, Hage Jr E. Influence of notching and molding conditions on determination of EWF parameters in polyamide 6. Polym Test 2004;23:195–202.
[28] Wu J-S, Mai Y-W, Cotterell B. Fracture toughness and fracture mechanisms of PBT/PC/IM blend: part I fracture properties. J Mater Sci 1993;28:3373–84.
[29] Maspoch MLl, Gámez-Pérez J, Gordillo A, Sánchez-Soto M, Velasco JI. Characterisation of injected EPBC plaques using the essential work of fracture (EWF) method. Polymer 2002;43:4177–83.
[30] Tjong SC, Xu S-A, Li RK-Y, Mai Y-W. Short glass fiber-reinforced polyamide 6,6 composites toughened with maleated SEBS. Compos Sci Technol 2002;62:2017–27.
[31] Wong SC, Mai Y-W. Essential fracture work of short fiber reinforced polymer blends. Polym Eng Sci 1999;39:356–64.
[32] Sui GX, Wong SC, Yue CY. The effect of fiber inclusions in toughened plastics-part I: fracture characterization by essential fracture work. Compos Sci Technol 2001;61:2481–90.
[33] Ching ECY, Poon WKY, Li RKY, Mai Y-W. Effect of strain rate on the fracture toughness of some ductile polymers using the essential work of fracture (EWF) approach. Polym Eng Sci 2000;40:2558–68.
[34] Luna P, Bernal C, Cisilino A, Frontini P, Cotterell B, Mai Y-W. The application of the essential work of fracture methodology to the plane strain fracture of ABS 3-point blend samples. Polymer 2003;44:1145–50.
[35] Karger-Kocsis J, Barany T, Moskala EJ. Plane stress fracture toughness of physically aged plasticized PETG as assessed by the essential work of fracture (EWF) method. Polymer 2003;44:5691–9.
[36] Karger-Kocsis J, Moskala EJ. Molecular dependence of the essential and non-essential work of fracture of amorphous films of poly(ethylene-2,6-naphthalate) (PEN). Polymer 2000;41:6301–10.
[37] Qiao Y, Avlar S, Chakravarthula SS. Essential fracture work of nylon 6-silicate nanocomposites. J Appl Polym Sci 2005;95:815–9.
[38] Mouzakis D, Karger-Kocsis J. Interrelation between energy partitioned work of fracture parameters and the crack tip opening displacement in amorphous polyester films. J Mater Sci Lett 2000;19:1615–9.
[39] Clutton E. In: Moore DR, Pavan A, Williams JG, editors. Fracture mechanics testing methods for polymer, adhesives and composites, ESIS 28. Amsterdam: Elsevier Science; 2001. p. 177–95.
[40] Wang Z, Liang Z, Wang B, Zhang C, Kramer L. Processing and property investigation of single-walled carbon nanotube (SWMT) buckypaper/-epoxy resin matrix nanocomposites. Composites Part A 2004;35: 1225–32.